Energy 68 (2014) 104–116

Contents lists available at ScienceDirect

Energy

journal homepage: www.elsevier.com/locate/energy

Numerical optimization of the occupancy rate of thermoelectric generators to produce the highest electrical power

Camille Favarel [a,b], Jean-Pierre Bédécarrats [a,*], Tarik Kousksou [b], Daniel Champier [b]

[a] Université Pau & Pays Adour, LaTEP – EA 1932, Laboratoire de Thermique, Energétique et Procédés, ENSGTI, Rue Jules ferry, BP 7511, Pau Cedex F-64075, France

[b] Université Pau & Pays Adour, Laboratoire des Sciences de l'Ingénieur Appliquées à la Mécanique et au Génie Electrique (SIAME), Hélioparc 2, Avenue du Président Angot, Pau Cedex 64053, France

ARTICLE INFO

Article history:
Received 30 April 2013
Received in revised form
4 February 2014
Accepted 8 February 2014
Available online 17 March 2014

Keywords:
Numerical simulation
Occupancy rate
Power generation
Thermoelectric generator

ABSTRACT

The electric power generated by thermoelectric modules obviously depends not only on the nature of the modules but also on heat transfers on both sides of these modules. In addition to the improvement of the thermoelectric material and module, analysis of thermoelectric systems is equally important in achieving their high-performance.

The aim of this study is to investigate the electric power extractable from a system equipped with thermoelectric modules and the influence of operating parameters on electricity generation. A computer model was developed to simulate the performances of the thermoelectric system. The influence of the position of the thermoelectric couples (occupancy rate) along the system was studied in order to optimize electrical power. The results obtained for modules made with Bi_2Te_3 from two various data sources and with slightly different thermoelectric properties are also presented in the study. Another study was made for automotive application. In this case, the use of various types of modules was considered. In each case the numerical model shows the importance of the repartition and choice of thermoelectric couples. It shows that for each thermoelectric fabrication there is an optimal occupancy rate which can vary greatly.

1. Introduction

TE (thermoelectric) devices directly convert thermal power to electrical power (Seebeck effect) and the opposite, electrical power to thermal power (Peltier effect).

Much research in recent years has focused on thermoelectricity to produce electricity. TEGs (TE generators) offer advantages such as high reliability, silence and low environmental impact and can use amounts of waste heat as an energy source in a simple and easy manner. Even if it has low energy conversion efficiency of around 2–5%, this technology is simple, robust, and has no moving parts [1]. Moreover, low efficiency is no longer the major issue when waste heat is recovered as a low-cost heat source.

Applications of TE generators are various. It is, for example, the case in the development of autonomous and maintenance-free sensors [2]. In both industrial processes and transportation, thermoelectricity can be used to exploit dissipated waste heat as electricity. The recovery of this waste heat (mainly exhaust gases), also known as energy harvesting, by means of thermoelectric generators is set to make a key contribution to the more efficient use of energy in the future [3].

Another attractive option is for providing small amounts of electricity to homes in developing countries, where currently about 1.6 billion people lack access to electricity [4,5].

TEGs are also used for cogeneration systems [3–5]. The goal in this case is not only to use heat to generate electricity but also for another objective, for example to produce hot water.

TEGs have many possible objectives but to be used industrially in a more efficient way, it is necessary to optimize them taking into account the specific features of each application.

In a classical thermoelectric generator, a heat exchanger captures the heat from the hot source and transfers this heat to the thermoelectric elements while another heat exchanger evacuates heat to a cold source in order to have a significant temperature gradient between the two faces of the TE elements. Various parameters affect the efficiency of a thermoelectric generator.

The main work consists in predicting the performance of TEGs with a particular configuration of heat exchangers and in studying

* Corresponding author. Tel.: +33 (0)559407717; fax: +33 (0)559407740.
E-mail address: jean-pierre.bedecarrats@univ-pau.fr (J.-P. Bédécarrats).

http://dx.doi.org/10.1016/j.energy.2014.02.030
0360-5442/

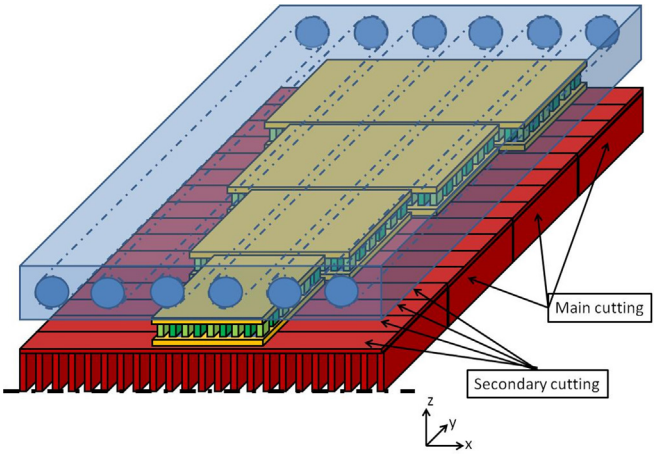

Fig. 1. Schematic diagram of the modelled thermoelectric generator (not in scale).

the effect of fluid flow rates, fluid properties and inlet temperatures on the power supplied by the system.

Numerous experimental studies [6,7] showed the influence of flow patterns, hot and cold temperatures, numbers of modules and geometry of the heat exchanger. The results obtained depend on the modules used, the type of heat exchanger and the operating conditions. So it seems pertinent to use modelling in order to optimize the whole thermoelectric system.

Most of the models combine the heat transfer equations and the standard thermoelectric equations including the Seebeck effect, Fourier effect and Joule effect. These models are qualified as standard models. Using this type of model, many studies [8] were carried out to simulate, for example, the type of heat exchangers [9–12], a specific geometry for aeronautics [13] and automotive [14] applications. Some numerical studies incorporate the Thomson effect [15–19] and show that this model is more accurate. For example, Nguyen and Pochiraju [20] solved a transient thermoelectric model that includes Seebeck, Peltier, Thomson, and Joule effects using finite-difference techniques to simulate the power generated from a TEG. The results showed that adding the Thomson effect plays a significant role in accurately predicting the power generated by the device. However, for optimization, the standard model is still good enough to obtain good accuracy and low calculation time.

TE material properties and heat exchanger performance are closely linked. When the variation of temperature is significant, the use of various types of TE modules is pertinent. For example, for temperatures above 330 °C, bismuth telluride becomes damaged. Espinosa et al. [21] studied a simple thermoelectric architecture composed of Mg_2Si/Zn_4Sb_3 (high temperature) followed by bismuth telluride materials (low temperature) along a given heat exchanger. They investigated the ideal proportion of required high-temperature materials. The number of thermoelements and electrical connections was addressed as well. Relevant engine operating points on a typical truck duty cycle were used as inputs in calculations to match actual engine conditions. They also discussed the influence of the connection of the module, presenting the case of all modules connected in series and then all modules connected separately. Kumar et al. [22] designed various efficient heat exchangers for automotive application also using a hybrid configuration (combination of bismuth telluride and skutterudite modules) to increase the system's electrical power output for the given thermal profile inside the TEG.

Although the interest of modelling in comprehension of the phenomena was demonstrated, little attention has been paid to the real optimization of the TEG.

Some optimizations have already been performed [23–25] but they do not take into account variations of the thermoelectric properties with temperature, whereas they could be significant under certain conditions.

The present paper focuses on a numerical study for optimizing the electric power extractable from a system equipped with thermoelectric modules. This system is a TEG whose hot source is a gas stream and whose cold source is a moving liquid. It was designed with typical configuration to easily understand the factors influencing TEG efficiency.

The electric power generated by TE modules obviously depends not only on the properties of the modules but also on heat transfers on both sides of these modules. So the position of the TE modules in the systems has an influence on electricity generation.

Some of our first results have already been presented [26] on the positioning of thermoelectric generators in order to produce the highest electrical power. The preliminary numerical results obtained for Bi_2Te_3 modules from two different data sources and with slightly different thermoelectric properties showed that the output electrical power is sensitive to the number and position of TE modules on the surface area of the heat exchanger. But these first

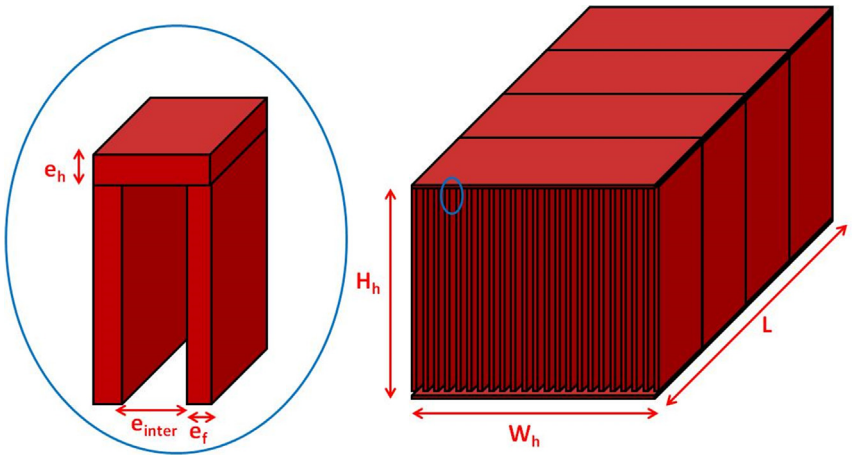

Fig. 2. Geometry of the hot heat exchanger.

results have to be confirmed by a new study improving the model and its optimization.

In this new paper, the full analyses of our numerical work are detailed, highlighting recent developments which have never been presented. Particular attention is paid to the position, number and type of TE modules along the system.

The computer model is developed to simulate performances of the designed TE system under various conditions of use. The results are presented in two cases. The first one corresponds to conditions that will be obtained in a future experimental loop and the second to conditions for automotive waste heat recovery.

In the first case, the results obtained for various modules made with Bi_2Te_3 are presented. For automotive application, the use of various materials (PbTe TE modules and Bi_2Te_3 TE modules) for the TEG is studied.

2. Geometry and description of materials

The geometry of the whole system was chosen to numerically study an experimental device which is under construction and will be tested in the near future. It consists in TE modules sandwiched between a hot fin heat exchanger and a cold heat exchanger (Fig. 1). The whole system is symmetrical along the x, y plane in order to reduce the calculation time. The used hot gas is air. The used liquid is glycol water. The model can simulate other fluids if necessary modifying its thermal properties.

2.1. Hot heat exchanger

The hot heat exchanger (Fig. 2) collects and transfers the thermal power from the hot gas stream through the TE modules. It is built with an assembly of fins (thickness e_f) separated by a space e_{inter}. The thickness of the base of the exchanger is e_h. The global dimensions of the exchanger are given in Table 1. It is made of 6063 aluminium. Hot gas (air) circulates inside this tube.

2.2. Cold heat exchanger

It is a tubular aluminium heat exchanger with an inner diameter of D_c and a thickness of e_c. The geometry is given in Fig. 3 and the dimensions in Table 2.

2.3. Thermoelectric modules

The TE modules represented in Fig. 4 are made up of 3 parts. On the top and bottom, ceramic layers (thickness e_{ceram}) form the electrical insulation. Between these two layers, the TE couples consist in two legs of n- and p-type doped semiconductor materials. The area and the length of the legs are respectively S and l for each type. The dimensions are given in Table 3. Air is present between the couples. The electrical connections are in metal. Several types of TE modules can be used. The density of the couple is defined by the ratio of the area occupied by the TE couple to the area occupied by the module. This value of the density is chosen to take into account the electrical insulation as well as the mechanical resistance. The modules used have a density fixed at 0.5518 according to the manufacturer 1 [27]. The TE properties depend on the materials used and also on the temperature.

Table 1
Dimensions of the hot heat exchanger.

Dimension	Symbol	Value
Height	H_h	0.118 m
Length	L	Depends on the study
Width	W_h	Depends on the study
Fin thickness	e_f	1.56 mm
Thickness of the exchanger walls	e_h	0.01 m
Distance between adjacent fins	e_{inter}	0.004 m

Table 2
Dimensions of the cold exchanger.

Dimension	Symbol	Value
Length	L	0.224 m
Width	W_c	Depends on the study
Thickness of the tube	e_c	0.006 m
Diameter of the tubes	D_c	0.014 m

3. Physical modelling

The physical model of the TEG was made under the following assumptions:

- Only the steady state case is considered;
- Fluid flows are considered unidirectional;
- Hot and cold fluid flows are incompressible and Newtonian;
- The conduction along the flow direction is negligible;
- All the TE modules are composed of a single layer of p–n junctions as illustrated in Fig. 4;
- The electrical contact resistance between the p and n couples is assumed to be negligible;
- The material properties for the TE couples vary along the length of the exchanger with changes in temperature;
- A simplified model of the cold exchanger has been implemented in order to reduce the calculation time. The change in temperature of the cold fluid is very low.

The description of the TEG involves multiple physical models, combining heat transfers, fluid mechanics, TE equations and electricity.

The TEG is cut into four main surfaces. In each main surface, both the occupancy rate and current of the TE modules can be chosen separately.

The occupancy rate τ is defined for each main surface as the ratio of the area occupied by the TE modules (S_i) on the area of the heat exchanger ($S_H = W.L/4$). It is illustrated in Fig. 5.

Then, for better accuracy, each main surface is cut into four secondary surfaces where all the equations are solved.

3.1. Heat transfers

Using these assumptions, the governing equation to describe the energy balance equations at steady state for the hot fluid and the cold fluid is as follows:

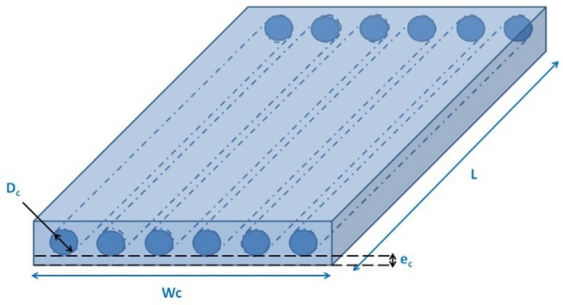

Fig. 3. Geometry of the cold heat exchanger.

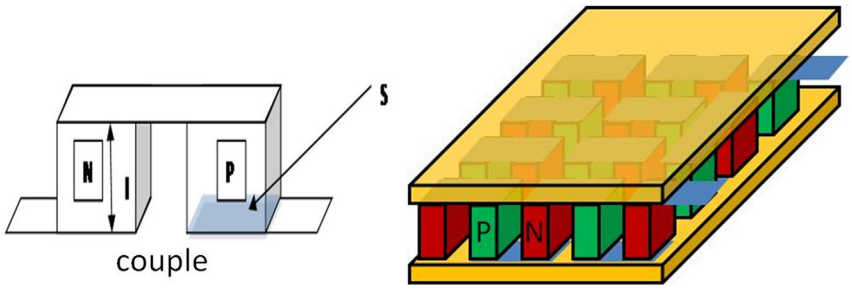

Fig. 4. TE couple/TE module.

$$\rho_H c_{p,H} u_H \frac{\partial T_H}{\partial y} = \frac{-Q_H}{V_H} \quad (1)$$

$$\rho_C c_{p,C} u_C \frac{\partial T_C}{\partial y} = \frac{Q_C}{V_C} \quad (2)$$

where ρ, C_p, u and T respectively represent the density, specific heat capacity, velocity and temperature of the fluid. V is the volume occupied by the fluid. The subscripts C and H correspond to the cold and hot fluid. Q_C is the heat flux transferred between the cold fluid and the TE modules and Q_H the heat flux transferred between the hot fluid and the modules. y corresponds to the position along the heat exchanger.

Six temperatures are calculated in each control volume (Fig. 6): the hot and cold fluid temperatures (T_H and T_C), the hot and cold wall surface temperature ($T_{H,wall}$ and $T_{C,wall}$) and the hot and cold side temperature of the couple ($T_{H,couple}$ and $T_{C,couple}$). For this purpose, an equivalent electrical model using thermal resistances for each secondary surface (subscribe k) is built as illustrated in Fig. 7.

$R_{H,conv}$ and $R_{C,conv}$ are the thermal convective resistances. $R_{H,cond}$ and $R_{C,cond}$ are the thermal conduction resistances of the exchanger. R_{air} is the thermal resistance of the air sandwiched between the hot and cold exchangers. $R_{H,ceram}$ and $R_{C,ceram}$ are the thermal conduction resistances of the ceramic materials. R_{couple} is the thermal conduction resistance of the TE couples. R_{is} is the thermal resistance of the insulated material between the TE couples.

$R_{H,ctc}$, $R_{C,ctc}$ represent the thermal contact resistances between the ceramic layers and the heat exchanger material, and between the ceramic layers and the TE couple on each side of the modules. A constructor datasheet [28], which takes into account the pressure applied on the TE modules, is used to calculate them.

The solution is then found using a Newton–Raphson method for nonlinear equations.

3.2. Fluid flow part

In order to calculate the thermal convective resistances, the following heat transfer coefficients h_H and h_C have to be calculated. They are given by the next formula:

$$h = \frac{kNu}{L_c} \quad (3)$$

Table 3
Dimensions of a thermoelectric couple.

Symbol	Definition	Value
l	Length of a couple	$1.8\ 10^{-3}$ m
S	Surface of a couple	$(2.6\ 10^{-3})^2$ m^2

where k is the thermal conductivity of the fluid, L_c is the characteristic dimension. The Nusselt number Nu is calculated using heat transfer correlations.

Empirical correlations for the hot side (air) and cold side (liquid water with 30% glycol content) convective heat transfers are implemented for the heat exchanger models. The different correlations depend on the flow regime (laminar, transient or turbulent). The selected correlations are valid for fully developed pipe flow.

When the Reynolds number is $Re < 2300$, the flow is laminar and the Shah and London correlation [29] is used to predict the mean Nusselt number Nu. For the hot fluid flow through the inner tube, $Nu = 7.5$ and for the cold fluid, $Nu = 4.363$.

The Gnielinski correlation [30] is used in the range $2300 \le Re \le 5 \times 10^6$ (transient and turbulent):

$$Nu = \frac{\left(\frac{f}{2}\right)(Re - 1000)Pr}{\left[1 + 12.7\left(\frac{f}{2}\right)^{0.5}\left(Pr^{0.66} - 1\right)\right]} \quad (4)$$

$$\text{With : } f = \frac{1}{[1.58 \times \ln(Re) - 3.28]^2} \quad (5)$$

f is the fanning friction factor. Pr the Prandtl number is in the range $0.5 \le Pr \le 10^6$.

Because of the rectangular cross-section and the presence of fins, the hydraulic diameter is used in each correlation.

3.3. Thermoelectric part

The one dimensional model commonly described in literature (1-D heat flow) for a typical TE module made of n thermocouples [1] is used.

These equations are derived from the study of a single n- or p-type element assuming that all connections between the elements are perfect: no electrical and thermal resistance.

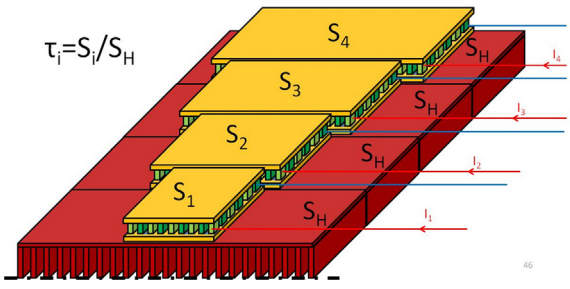

Fig. 5. Definition of the occupancy rate.

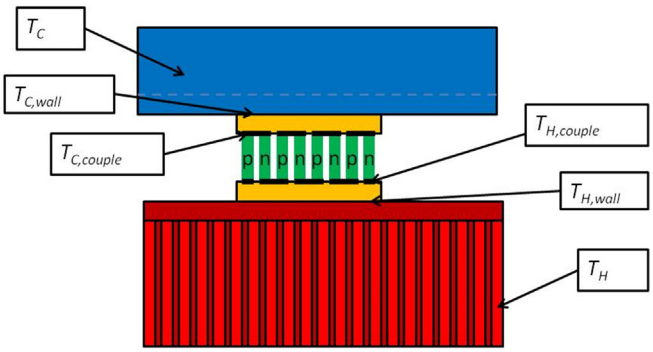

Fig. 6. Geometry of the thermoelectric generator.

The TEG is well insulated (no heat exchange with the surroundings).

Energy balance around the TE modules leads to the following equations for the hot side heat flux Q_H into the TE modules, the cold side heat flux Q_C out of the TE modules and the electric power P_e:

$$Q_H = n\left[\alpha(T)I\ T_{H,couple} - \frac{R_{elec}(T)I^2}{2} - \frac{T_{C,couple} - T_{H,couple}}{R_{couple}(T)}\right] \quad (6)$$

$$Q_C = n\left[\alpha(T)I\ T_{C,couple} + \frac{R_{elec}(T)I^2}{2} - \frac{\left(T_{C,couple} - T_{H,couple}\right)}{R_{couple}(T)}\right] \quad (7)$$

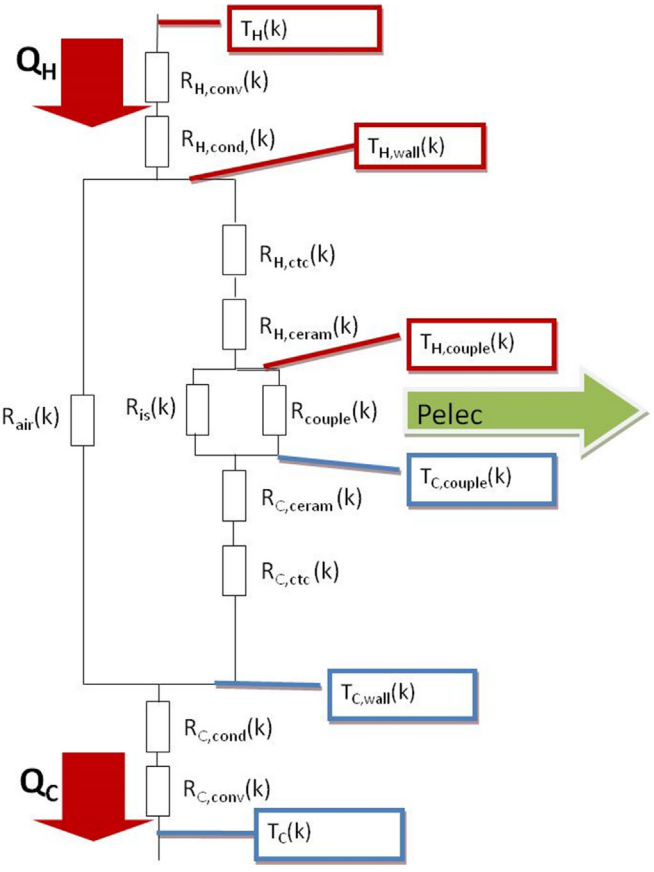

Fig. 7. Thermal resistances model of the thermoelectric generator.

Table 4
Main parameters used by the GA.

Size of the population = 200
Number of generations = 200
Crossover rate = 0.5
Mutation rate = 0.07

$$P_e = Q_H - Q_C = n\left\{\alpha(T)I\left[T_{H,couple} - T_{C,couple}\right] - R_{elec}(T)I^2\right\} \quad (8)$$

where α, R_{elec} and R_{couple} are respectively the Seebeck coefficient, the electrical resistance and the thermal resistance of a single thermocouple which are functions of the average temperature $T = (T_{H,couple} + T_{C,couple})/2$. $T_{H,couple}$ and $T_{C,couple}$ are respectively the temperature of the hot side and cold side of the legs. In each main surface, the TE couples are wired in series so they have the same current. I is the electrical current through a single thermocouple.

This current I is a parameter of our model and is used to obtain the maximum electrical power.

3.4. Global thermoelectric model

Using the previous assumptions, the whole TEG has been simulated with the language and interactive environment Matlab. A function including all the previous equations has been implemented. The main input arguments of this function are the size of the heat exchangers (Tables 1 and 2), the cold and hot flow rates, the inlet cold and hot fluid temperatures, the TE material properties, the electrical currents and the occupancy rates for each main surface. The electrical power, the open voltage, the internal resistance and all the thermal parameters, such as temperatures and fluxes, are calculated for each main surface and for the TEG. The TEG total efficiency is also calculated.

4. Optimization

The objective of the optimization is to maximize the electric power extractable from the presented system (Section 2), for different temperatures and flow rates of the fluids.

The first study focuses on the influence of the number of TE modules (occupancy rate) – in each control volume – along the fixed geometry of the heat exchanger, and on the influence of the electrical currents. The occupancy rates can vary from 0 to 100%. The values of the electrical currents can vary from 0 to 20 A. This higher value corresponds to the highest current acceptable for the used TE modules. In practice, the value of the currents can be set with DC/DC converters.

In a second study, another degree of freedom, the TE properties, is added in order to investigate the mixing of different TE materials.

Given these considerations, the electrical output power determined by the model (Section 3.4), is chosen as the objective function.

The retained optimization strategy is a GA (genetic algorithm), because it is robust and easily transferable to existing simulations

Table 5
Geometry of the parametric analysis.

Symbol	Definition	Value
W_H	Width	0.112 m
W_C	Width	0.112 m
L	Length	0.224 m
Ncut	Number of secondary areas	4

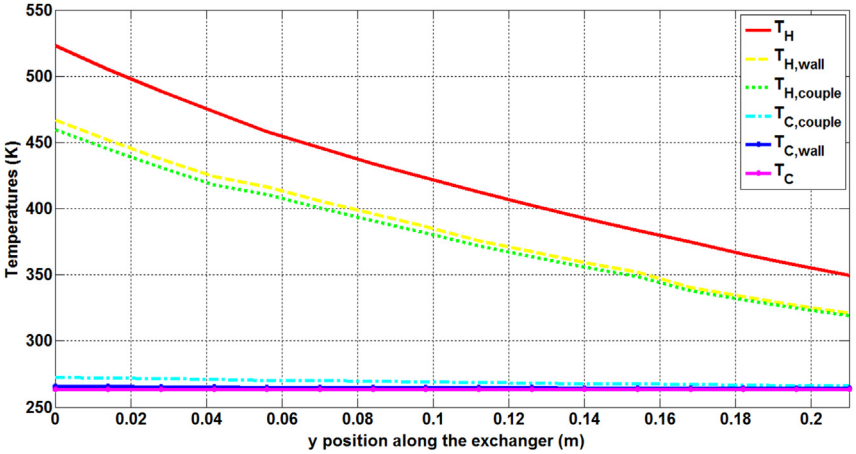

Fig. 8. Temperatures profiles along the exchanger in the optimized case.

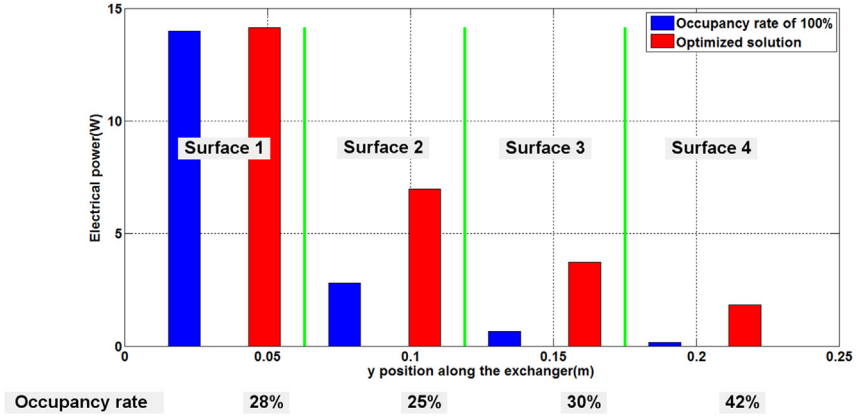

Fig. 9. Electrical power per area for $T_H = 250$ °C. Airflow rate = 21 m^3 h^{-1}.

and models. The GA is a method of stochastic optimization inspired by biological evolution [31,32].

The GA considered here used real numbers and was elitist. Crossover children are created by combining the vectors of a pair of parents. The used crossover operation is the blend crossover operator (BLX-α). Mutation children are created by introducing random changes, to a single child, a uniform mutation over the entire domain for occupancy rate genes and a local mutation for the current genes is used.

The GA was tested to determine their convergence rate and prevent illogical divergence. The main settings of the GA are summarized in Table 4.

The electrical output power is calculated for each individual in the population. A tournament selection is made: 50% of the

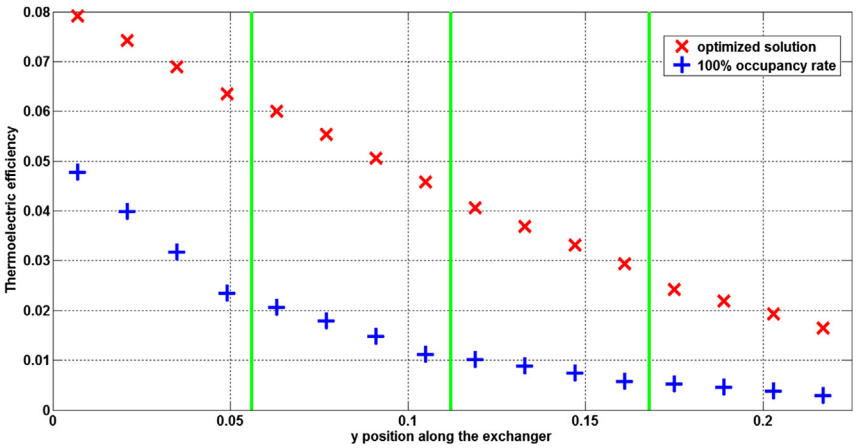

Fig. 10. TE efficiency for $T_H = 250$ °C. Airflow rate = 21 m^3 h^{-1}.

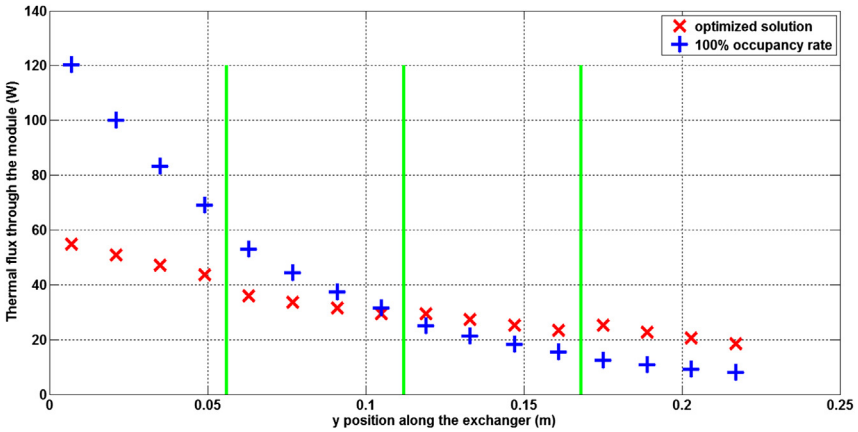

Fig. 11. Thermal flux for $T_H = 250\ ^\circ C$. Airflow rate = 21 $m^3\ h^{-1}$.

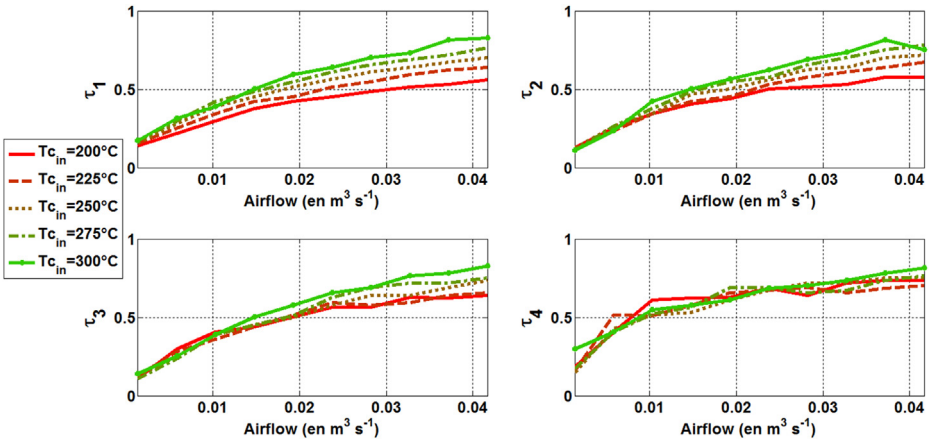

Fig. 12. Optimized occupancy rates of the exchanger with Bi_2Te_3 of manufacturer 1 [23].

population is selected by a criterion corresponding to the highest electrical output power and a crossover between the populations is made to generate the other 50% of the next generation. After that the mutation is performed.

After 200 generations, the genetic algorithm gives its best solution. That is to say that the convergence was declared when the improvement of the objective function was less than 0.1% during 200 consecutive generations. At this stage, the Matlab optimization function [33] is used to find the local maximum.

The GA is a probabilistic method; two runs with the same settings can potentially lead to two different results (different local minimum/maximum). Therefore we performed four optimization runs with the GA for each test case considered in order to ensure the repeatability of the results. Only the best result

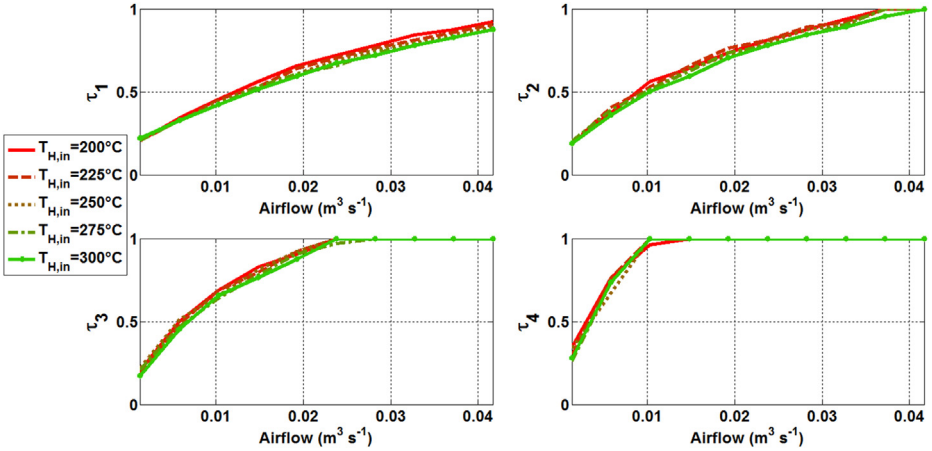

Fig. 13. Optimized occupancy rates of the exchanger with Bi_2Te_3 of manufacturer 2 [24].

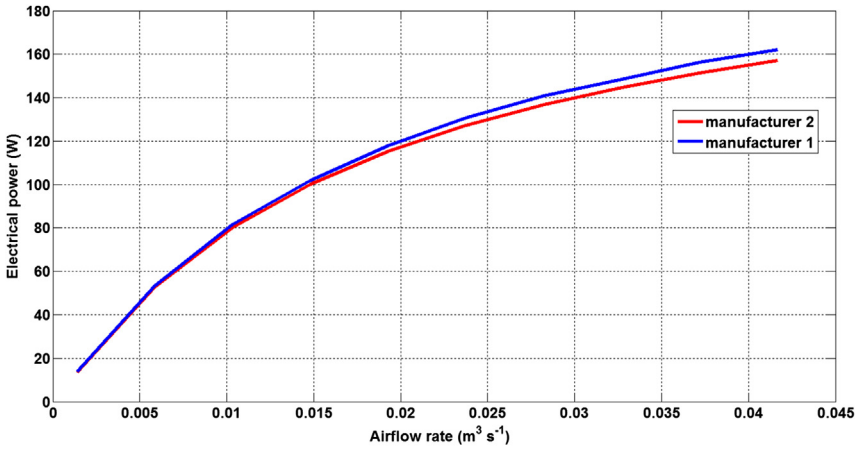

Fig. 14. Comparison of the electrical power produced by the two manufacturers for $T_{H,in} = 250$ °C.

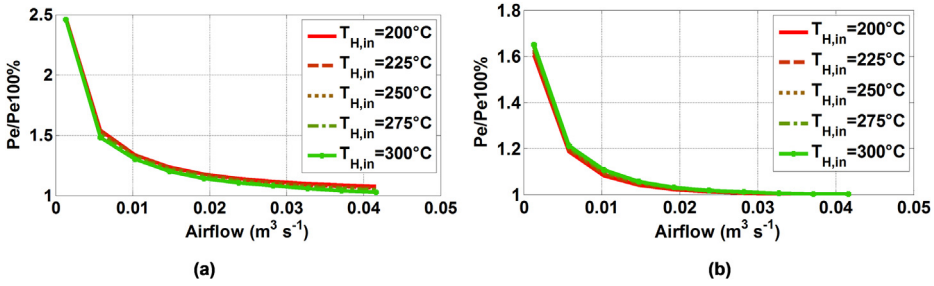

Fig. 15. Electrical power ratio for (a) manufacturer 1 and (b) manufacturer 2.

among the four runs was retained and was presented in this work.

5. Simulation results and discussions

In the following numerical simulations, the TE properties of two different TE materials, Bi_2Te_3 and PbTe, are used [34–36]. Bi_2Te_3 properties are from manufacturer 1 and manufacturer 2 and PbTe properties are only provided by manufacturer 1. Generated electrical power, thermal power through the modules, TE efficiency, and occupancy rate are calculated. For each optimization, two electrical powers, Pe and Pe100%, are evaluated for a fixed couple (inlet hot fluid temperature, airflow rate). Pe is obtained by simultaneously optimizing the occupancy rate and the currents through the modules. Pe100% is obtained by covering the entire area with modules and by only optimizing the currents.

5.1. Parametric analysis

First of all, the different simulations show that the temperature of the cold side of the heat exchanger hardly varies. The high values

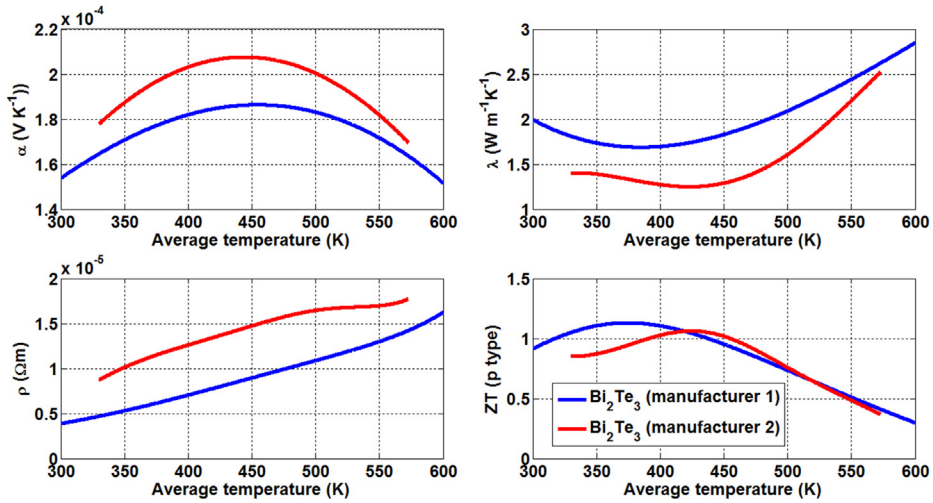

Fig. 16. Thermoelectric characteristics and ZT of p types.

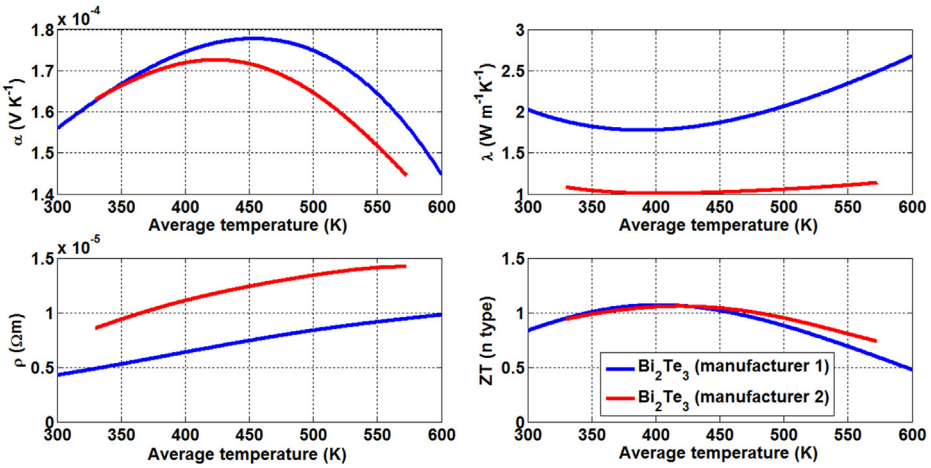

Fig. 17. Thermoelectric characteristics and ZT of n types.

of the specific heat of the fluid (water with 30% of monoethylene glycol) and of the considered flow ranges easily explain this result.

The first optimization is the maximization of electrical output power for different conditions of the hot fluid (airflow rate – inlet temperature) and for the two different Bi_2Te_3 modules. For the cold fluid, the inlet temperature is set at −10 °C and the flow rate is 10 $m^3\ h^{-1}$. The geometry of the studied heat exchanger is given in Table 5.

The first study focuses on the optimization for a specific point with an air inlet temperature of 250 °C and an airflow rate value of 21 $m^3\ h^{-1}$.

Fig. 8 shows the temperature profiles along the exchanger in the optimized case. We can see that the hot temperature decreases rapidly whereas the cold one is almost constant. This is the result of the difference in the values of product $\rho \cdot C_p$ which is much higher in the case of the cold fluid. The temperature difference between the fluid and the wall is more significant for the hot side due to high convection resistance of the hot fluid (air). Exchanges are better on the cold side thanks to the nature of the fluid.

The electric power produced by the exchanger and the occupancy rate are presented in Fig. 9. The red (in web version) bars correspond to the optimized solution and the blue (in web version) ones to the case where the whole area of the exchanger is covered by modules.

TE efficiency, which is defined by the ratio of electrical power produced over the hot thermal flux through the modules, is presented in Fig. 10. The corresponding hot thermal flux through the modules is presented in Fig. 11.

In the optimized case (coloured red), as there are less TE materials, the total thermal resistance between the hot and cold exchangers is greater. So the temperature difference is higher. As efficiency is a function of temperature difference, it is higher in the optimized case. With the 100% occupancy rate, the collected thermal flux is higher so the temperature of the hot fluid decreases faster along the exchanger. The result is a significant decrease in TE efficiency in areas 2, 3 and 4 which is directly connected to the temperature difference. The 100% occupation rate favours the thermal flux of each area separately. It results in a quick decrease of the thermal flux along the exchanger.

The optimized electrical power and the 100% occupancy rate of the fourth area are presented in Fig. 9. With the 100% occupancy rate, a negligible electrical power is obtained after the second area. Thanks to optimization of the occupancy rate, the decrease in temperature is slower and TE efficiency is better. Moreover, the thermal flux available for the last areas is higher. In the optimized occupancy rate case, the total electric power is about 51 W whereas this power is only 35 W in the 100% occupancy rate case. The benefit of optimization is almost 1.5.

For the optimized solution, these last three figures traduce the competition between having high efficiency (high temperature difference) with a low thermal flux (high thermal module resistance) and having a high thermal flux (low thermal module resistance) but low efficiency (low temperature difference). The maximum electrical power is obtained for the optimized case between these two goals.

The second study is a generalization of these results when the flow rates and temperatures of the hot air vary.

Fig. 12 presents the optimized occupancy rate of the different parts of the exchanger for modules from manufacturer 1 for different inlet temperatures of the hot fluid $T_{H,in}$. τ_1 corresponds to the first main area at the inlet of the heat exchanger and τ_4 is the last one at the outlet. At low airflow rate, the occupancy rates are low, and the impact of the hot temperature is negligible for all the areas. For intermediate airflow rate, the inlet temperature of the hot fluid has a small impact on the first area, but becomes less significant for the following areas. For high airflow rate, the impact is higher and stays significant for the first three areas. The inlet temperature of the hot fluid just has an influence on the thermal power available and the efficiency, therefore the more we advance along the exchanger, the less it impacts. Indeed, for the final surfaces, the increase in the thermal power due to the hot inlet

Table 6
Geometry of the multi material analysis.

Symbol	Definition	Value
W_H	Width of the hot exchanger	0.336 m
W_C	Width of the cold exchanger	0.336 m
L	Length	0.448 m
Ncut	Number of secondary areas	8

Table 7
Materials used in the multi material analysis.

Materials	Symbol
Bi_2Te_3	Bi_2Te_3 [33]
Bi_2Te_3	Bi_2Te_3 [34]
PbTe	PbTe [35]

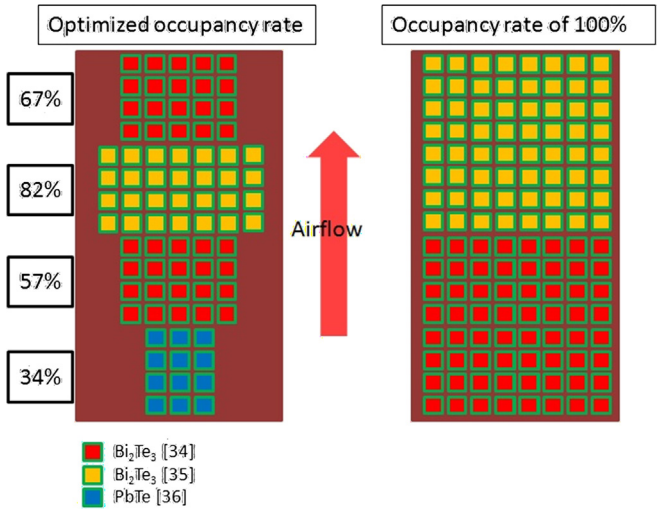

Fig. 18. Material optimization.

temperature no longer has an impact because the temperature has dropped in the previous surfaces.

Fig. 13 shows the same study with the second manufacturer. It appears that the hot inlet temperature has no impact on the optimized occupancy rate. For the entire airflow rate intervals, the optimized occupancy rate grows with the position along the exchanger as illustrated in Fig. 5. The number of modules increases along the exchanger. Another phenomenon is seen with the saturation of the occupancy rate. At high airflow rate, almost all the areas are completely covered.

These two figures also demonstrate that for a fixed hot inlet temperature, the optimized occupancy rates grow with airflow rate. This is logical. Increasing the airflow not only increases the available thermal power but also decreases the thermal convection resistance. This second point increases the occupancy rates without degrading temperature difference and therefore without degrading efficiency.

Fig. 14 presents the electrical power produced for the two manufacturers as a function of the airflow rate. This result is given for $T_{H,in} = 250$ °C. The electrical powers are similar for low airflow rates and are slightly different for high ones. The small difference is due to the saturation of the occupancy rate in the case of the second manufacturer. Indeed when the occupancy has reached 100% we can no longer use this parameter to optimize.

It is possible to define an electrical power ratio (Pe/P100%) which is the ratio between the electrical power generated with the optimized solution Pe over the electrical power generated by the 100% occupancy rate solution Pe100%. This ratio shows the significant difference between the two manufacturers.

Fig. 15 shows the evolution of this ratio with the airflow rate and clearly demonstrates the interest of optimization. The results show that the choice of an occupancy rate of 100% is awkward especially for low airflow rates. For an airflow rate of 0.006 $m^3\ s^{-1}$, a benefit in power of 20% is achieved with manufacturer 2 and even of 50% with manufacturer 1.

To understand the differences between the two manufacturers, the different TE characteristics for the n- and p-type doped semiconductor materials are shown in Figs. 16 and 17.

The performances of TE materials are commonly compared using the dimensionless coefficients of merit named ZT and defined as $z_nT = \alpha_n^2/\rho_n\lambda_n$ and $z_pT = \alpha_p^2T/\rho_p\lambda_p$, where α_n, ρ_n, λ_n and α_p, ρ_p, λ_p are respectively, the Seebeck coefficient, the electrical resistivity, the thermal conductivity of the n- and p-type doped semiconductor materials.

It appears that the ZT coefficients are quite similar, but the other TE characteristics (Seebeck coefficients, specific resistances, thermal conductivities) are different. For the p-type doped material, the choice of doping of manufacturer 1 allows a higher Seebeck coefficient and a lower thermal conductivity. They contribute to increase ZT but the drawback is a higher electric resistivity that decreases ZT. For the n-type doped material, the choice of doping by the manufacturer favours mainly the thermal conductivity at the expense of the electrical resistivity.

It can be seen from Fig. 14 that the two types of modules that have substantially the same ZT coefficients provide the same electric power. On the contrary, the optimal occupancy rate is not connected to the ZT coefficients. The occupancy rate is connected to the other parameters and probably mostly to the thermal conductivity: the lower the thermal conductivity, the higher the optimal occupancy rate.

5.2. Multi-materials analysis

The second optimization is the maximization of electrical output power in a specific condition corresponding to automotive application. The airflow rate and the water flow rate are set respectively at 420 $m^3\ h^{-1}$ and 10 $m^3\ h^{-1}$, and the hot and cold inlet temperatures are set respectively at 620 °C and 80 °C. This study is built on the comparison of two different optimizations. In the first case we optimize the global electrical power varying the occupancy rates, currents and materials on the four main areas. In the second case the occupancy rate is set at 100% and the global electrical

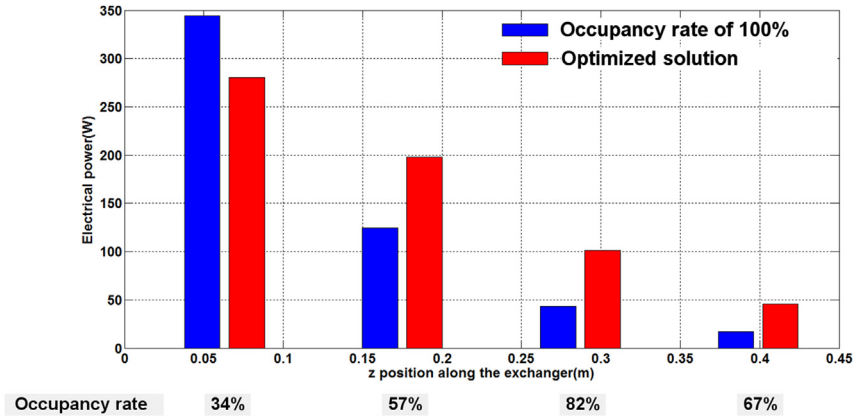

Fig. 19. Comparison of the electrical power along the exchanger.

power is optimized varying the currents and materials on each main surface. The choice of different materials is based on the industrial maturity of the module. Only modules available on the market are considered. The geometry of the exchanger and the TE materials used are respectively given in Tables 6and 7.

Fig. 18 shows the positioning of different TE materials obtained by optimization. The optimized solution uses the three TE materials with four different occupancy rates. Fig. 19 shows the comparison of the electrical powers obtained in both cases. Fig. 20 shows the temperature profiles along the exchanger in the optimized occupancy rate case (a) and in the occupancy rate of 100% case (b).

Comparing Fig. 20a and b clearly shows that the hot air temperature decreases much faster in the 100% occupancy rate case whereas in the optimized solution the temperature remains at a higher level for a longer distance. It can also be noticed that the major part of the temperature losses is located in the hot exchanger (thermal convection resistance). The optimized solution always provides a more significant temperature difference ($T_{H,couple} - T_{C,couple}$) and, therefore, better use of the wasted thermal energy.

The electrical power generated by the optimized solution is 1250 W which is about 18% higher than the 100% occupancy rate solution which produces 1059 W. For the 100% occupancy rate case, only the first main area produces more electrical power. But absorbing too much thermal energy has serious consequences; it decreases the temperature difference for the next three surfaces which dramatically decreases TE efficiency as it has already been explained in Section 5.1. It can be noticed that the optimization algorithm did not choose the PbTe material. Indeed, PbTe modules installed on 100% of the first main area would have taken a lot of thermal power and the temperature would have decreased too quickly. As for the optimized occupancy rate, it is possible to interpret the choice of the materials for each main surface. A few PbTe couples are used at the inlet of the exchanger because of their better efficiency at high temperature (see Fig. 20). On the second main surface, Bi_2Te_3 from manufacturer 1 is used even if it is not the most efficient. The reason is that the temperature is too high for the materials used by manufacturer 2. On the third surface, the temperature is low enough to use Bi_2Te_3 from manufacturer 2. On the final surface, Bi_2Te_3 from manufacturer 1 is more efficient, which is why it is chosen by the algorithm.

Another point of interest is the study of the link between the chosen materials and their figures of merit. For each secondary surface of the numerical mesh along the *y* axis, it is possible to calculate the average temperature and the corresponding ZTs. The result is presented in Fig. 21. It shows that optimization of the electric output power is equivalent to maximizing ZT along the exchanger. The singularity of the third surface is due to the maximum temperature accepted by manufacturer 2's TE material. This TE material cannot be used here even if it is more efficient. The limitation of the temperature forces the material with the best ZT not to be chosen by the algorithm.

6. Conclusion

As energy becomes more valuable and is increasingly required to be clean, energy recovery is one of the natural ways to answer

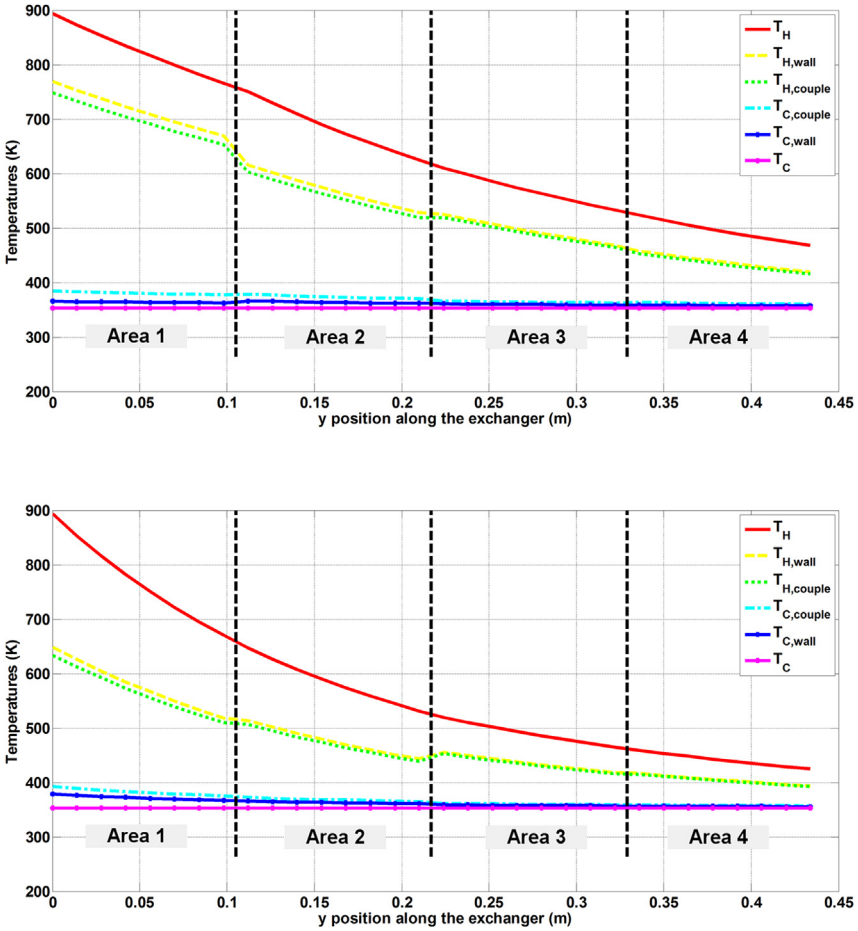

Fig. 20. Temperatures profiles (a) optimized solution, (b) 100% occupancy rate.

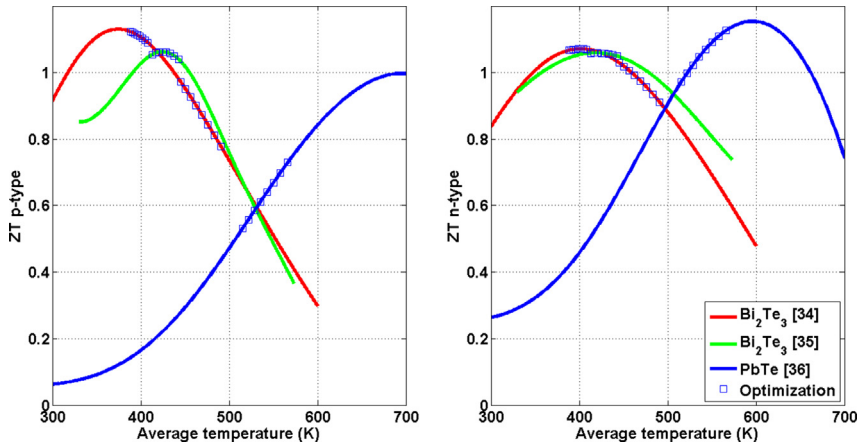

Fig. 21. Figure of merit of p and n type materials.

the problem. Specific attention is paid to recovering heat, which represents the major part of the losses. TEGs are one of the solutions. Nevertheless, due to their low efficiency, TEGs need to be optimized in order to be competitive.

In this work, the recovery of energy from a hot flowing gas is considered. A multiphysics model was built with numerous input parameters which take into account the variations of the thermodynamic properties with temperature. Moreover, a new parameter was introduced: the occupancy rate. A genetic algorithm was used to calculate the configuration which produces the maximum electrical power in various cases.

In the first study, one type of TE module was used and the electrical power was maximized by optimizing the occupancy rates and the electrical input currents. Initially, for a fixed hot air temperature and a fixed airflow rate, the maximum output electrical power was obtained for a configuration where TE modules do not completely cover the hot exchanger. The explanation of this result was given. These investigations had been extended to present the trends for different inlet hot air temperatures and different airflow rates. This extensive study focuses on two Bi_2Te_3 modules with different TE properties. It appeared that the electrical power produced in both case is comparable but the occupancy rates are different.

In a second study, the possibility of mixing the materials (Bi_2Te_3 and PbTe modules) was added for a specific operating point (automotive application) of inlet hot air temperature and airflow rate. The temperature constraints of the material were taken into account. Again, the results showed the interest of optimizing the TEG and the relevance of the occupancy rate parameter.

An experimental system has been built and tests are currently being carried out. The next step will be the comparison of the numerical and experimental results.

Acknowledgements

This work was carried out within the framework of a project whose objective is to study the feasibility of producing electricity with thermoelectric modules in various applications. It is funded in part by the Regional Council of Aquitaine and the General Council of Aquitaine (France).

References

[1] Riffat SB, Ma X. Thermoelectrics: a review of present and potential applications. Appl Therm Eng 2003;23:913–35.
[2] Francioso L, De Pascali C, Farella I, Martucci C, Cretì P, Siciliano P, et al. Flexible thermoelectric generator for ambient assisted living wearable biometric sensors. J Power Sources 2001;96(6):3239–43.
[3] Zheng XF, Yan YY, Simpson K. A potential candidate for the sustainable and reliable domestic energy generation – thermoelectric cogeneration system. Appl Therm Eng 2013;53:305–11.
[4] Champier D, Bédécarrats JP, Kousksou T, Rivaletto M, Strub F, Pignolet P. Study of a TE (thermoelectric) generator incorporated in a multifunction wood stove. Energy 2011;36(3):1518–26.
[5] O'Shaughnessy SM, Deasy MJ, Kinsella CE, Doyle JV, Robinson AJ. Small scale electricity generation from a portable biomass cookstove: prototype design and preliminary results. Appl Energy 2013;102:374–85.
[6] Chen WH, Liao CY, Hung CI, Huang WL. Experimental study on thermoelectric modules for power generation at various operating conditions. Energy 2012;45:874–81.
[7] Lesage FJ, Pagé-Potvin N. Experimental analysis of peak power output of a thermoelectric liquid-to-liquid generator under an increasing electrical load resistance. Energy Convers Manag 2013;66:98–105.
[8] Crane DT. An introduction to system-level, steady-state and transient modeling and optimization of high-power-density thermoelectric generator devices made of segmented thermoelectric elements. J Electron Mater 2011;40(5):561–9.
[9] Esarte J, Min G, Rowe DM. Modelling heat exchangers for thermoelectric generators. J Power Sources 2011;93(1–2):72–6.
[10] Yu J, Zhao H. A numerical model for thermoelectric generator with the parallel-plate heat exchanger. J Power Sources 2007;172:428–34.
[11] Jang JY, Tsai YC, Wu CW. A study of 3-D numerical simulation and comparison with experimental results on turbulent flow of venting flue gas using thermoelectric generator modules and plate fin heat sink. Energy 2013;53:270–81.
[12] Gou X, Yang S, Xiao H, Ou Q. A dynamic model for thermoelectric generator applied in waste heat recovery. Energy 2013;52:201–9.
[13] Kousksou T, Bédécarrats JP, Champier D, Pignolet P, Brillet C. Numerical study of thermoelectric power generation for an helicopter conical nozzle. J Power Sources 2011;196(8):4026–32.
[14] Kumar S, Heister SD, Xu X, Salvador JR, Meisner GP. Thermoelectric generators for automotive waste heat recovery systems. Part I: numerical modeling and baseline model analysis. J Electron Mater 2013;42:665–74.
[15] Meng F, Chen L, Sun F. A numerical model and comparative investigation of a thermoelectric generator with multi-irreversibilities. Energy 2011;36(5):3513–22.
[16] Sandoz-Rosado EJ, Weinstein SJ, Stevens RJ. On the Thomson effect in thermoelectric power devices. Int J Therm Sci 2013;66:1–7.
[17] Wee D. Analysis of thermoelectric energy conversion efficiency with linear and nonlinear temperature dependence in material properties. Energy Convers Manag 2011;52(12):3383–90.
[18] Fraisse G, Ramousse J, Sgorlon D, Goupil C. Comparison of different modeling approaches for thermoelectric elements. Energy Convers Manag 2013;65:351–6.
[19] Lee HS. The Thomson effect and the ideal equation on thermoelectric coolers. Energy 2013;56:61–9.
[20] Nguyen NQ, Pochiraju KV. Behavior of thermoelectric generators exposed to transient heat sources. Appl Therm Eng 2013;51:1–9.
[21] Espinosa N, Lazard M, Aixala L, Scherrer H. Modeling a thermoelectric generator applied to diesel automotive heat recovery. J Electron Mater 2010;39(9):1446–55.
[22] Kumar S, Heister SD, Xu X, Salvador JR, Meisner GP. Thermoelectric generators for automotive waste heat recovery systems. Part II: parametric evaluation and topological studies. J Electron Mater 2013;42:944–55.
[23] Suter C, Jovanovic ZR, Steinfeld A. A 1 kWe thermoelectric stack for geothermal power generation – modeling and geometrical optimization. Appl Energy 2012;99:379–85.

[24] Bélanger S, Gosselin L. Multiobjective genetic algorithm optimization of thermoelectric heat exchanger for waste heat recovery. Int J Energy Res 2012;36(5):632–42.
[25] Jang JY, Tsai YC. Optimization of thermoelectric generator module spacing and spreader thickness used in a waste heat recovery system. Appl Therm Eng 2013;51(1–2):677–89.
[26] Favarel C, Bedecarrats JP, Kousksou T, Champier D. The influence of operating parameters and occupancy rate of thermoelectric modules on the electricity generation. In: Proceedings of ECOS 2012-the 25th international conference on efficiency, cost, optimization, simulation, and environmental impact of energy systems June 26-29, 2012. Perugia, Italy.
[27] Technical data sheet. Thermonamic Products. http://www.thermonamic.com/TEHP1-12656-0.3-English.pdf [accessed 30.01.14].
[28] Technical data sheet. eGRAF® HITHERMTM Products. http://graftechaet.com/eGRAF/eGRAF-Technical-Documents.aspx [accessed 30.01.14].
[29] Rohsenow W, Hartnett J, Cho Y. Handbook of heat transfer. 3rd ed. McGraw-Hill Companies Incorporated; 1998.
[30] Gnielinski V. New equations for heat and mass transfer in turbulent pipe and channel flow. Int Chem Eng 1976;16:359–68.
[31] Goldberg DE. Genetic algorithms in search, optimization and machine learning. MA: Addison-Wesley Publishing Co. Inc.; 1989.
[32] Gosselin L, Tye-Gingras M, Mathieu-Potvin F. Review of utilization of genetic algorithms in heat transfer problems. Int J Heat Mass Transf 2009;52(9–10):2169–88.
[33] Lagarias JC, Reeds JA, Wright MH, Wright PE. Convergence properties of the Nelder-Mead simplex method in low dimensions. SIAM J Optim 1999;9(1):112–47.
[34] Technical data sheet. Thermonamic Products. http://www.thermonamic.com/Ingot%20specification%20sheet%20-English.pdf [accessed 30.01.14].
[35] Technical datasheet HiZ. http://www.hi-z.com/hz14.php [accessed 30.01.14].
[36] Technical data sheet. Thermonamic Products. http://www.thermonamic.com/PbTeIngotspecificationsheet-English%20version.pdf [accessed 30.01.14].